Direct observation of Gouy phase shift in a propagating optical vortex

Junichi Hamazaki, Yuriya Mineta, Kazuhiko Oka and Ryuji Morita

Department of Applied Physics, Faculty of Engineering, Hokkaido University, Kita-13, Nishi-8, Kita-ku, Sapporo 060-8628, Japan,

hamazaki@topology.coe.hokudai.ac.jp, morita@eng.hokudai.ac.jp

Abstract: Direct observation of Gouy phase shift on an optical vortex was presented through investigating the intensity profiles of a modified LG_p^m beam with an asymmetric defect, around at the focal point. In addition, the three-dimensional trajectory of the defect was found to describe a uniform straight line. It was quantitatively found that the rotation profile of a modified LG_p^m beam manifests the Gouy phase effect where the rotation direction depends on only the sign of topological charge m. This profile measurement method by introducing an asymmetric defect is a simple and useful technique for obtaining the information of the Gouy phase shift, without need of a conventional interference method.

OCIS codes: (350.1370) Berry's phase; (230.6120) Spatial light modulators; (999.9999) Optical vortices

References and links

1. L. Allen, M. W. Beijersbergen, R. J. C. Spreeuw, and J. P. Woerdman, "Orbital angular momentum of light and the transformation of Laguerre-Gaussian laser modes," Phys. Rev. **A45**, 8185–8189 (1992).
2. A. Ashkin, "Forces of a single-beam gradient laser trap on a dielectric sphere in the ray optics regime," Biophys. J. **61**, 569–582 (1992).
3. A. D. Mehta, M. Rief, J. A. Spudich, D. A. Smith, and R. M. Simmons, "Single-molecule biomechanics with optical methods," Science **283**, 1689–1695 (1999).
4. K. T. Gahagan and G. A. Swartzlander, Jr., "Optical vortex trapping of particles," Opt. Lett. **21**, 827–829 (1996).
5. T. Kuga, Y. Torii, N. Shiokawa, T. Hirano, Y. Shimizu, and H. Sasada, "Novel optical trap of atoms with a doughnut beam," Phys. Rev. Lett. **78**, 4713–4716 (1997).
6. E. M. Wright, J. Arlt, K. Dholakia, K. T. Gahagan, and G. A. Swartzlander, Jr., "Toroidal optical dipole traps for atomic Bose-Einstein condensates using Laguerre-Gaussian beams," Phys. Rev. A **63**, 013608-1–7 (2001).
7. J. Tempere, J. T. Devreese, E. R. I. Abraham, K. T. Gahagan, and G. A. Swartzlander, Jr., "Vortices in Bose-Einstein condensates confined in a multiply connected Laguerre-Gaussian optical trap," Phys. Rev. A **64**, 023603-1–8 (2001).
8. N. B. Simpson, K. Dholakia, L. Allen, and M. J. Padgett, "Mechanical equivalence of spin and orbital angular momentum of light: an optical spanner," Opt. Lett. **22**, 52–54 (1997).
9. L. Paterson, M. P. MacDonald, J. Arlt, W. Sibbet, P. E. Bryant, and K. Dholaki, "Controlled rotation of optically trapped microscopic particles," Science **292**, 912–914 (2001).
10. V. Garcés-Chávez, D. M. McGloin, M. J. Padgett, W. Dultz, H. Schmitzer, and K. Dholakia, "Observation of the transfer of the local angular momentum density of a multiringed light beam to an optically trapped particle," Phys. Rev. Lett. **91**, 093602-1–4 (2003).
11. A. Mair, A. Vaziri, G. Weihs, and A. Zeilinger, "Entanglement of the orbital angular momentum states of photons," Nature **412**, 313–316 (2001).
12. A. Vaziri, G. Weihs, and A. Zeilinger, "Experimental two-photon, three-dimensional entanglement for quantum communication," Phys. Rev. Lett. **89**, 240401-1–4 (2002).
13. G. Molina-Terriza, J. P. Torres, and L. Torner, "Management of the angular momentum of light: preparation of photons in multidimensional vector states of angular momentum," Phys. Rev. Lett. **88**, 013601-1–4 (2001).
14. K. Dholakia, N. B. Simpson, M. J. Padgett, and L. Allen, "Second-harmonic generation and the orbital angular momentum of light," Phys. Rev. A **54**, R3742–3745 (1996).

15. D. P. Caetano, M. P. Almeida, P. H. Souto Ribeiro, J. A. O. Huguenin, B. Coutinho dos Santos, and A. Z. Khoury, "Conservation of orbital angular momentum in stimulated down-conversion," Phys. Rev. A **66**, R041801-1–4 (2002).
16. A. Vinçotte and L. Bergé, "Femtosecond optical vortices in air," Phys. Rev. Lett. **95**, 193901-1–4 (2005).
17. D. Neshev, A. Nepomnyashchy, and Y. S. Kivshar, "Nonlinear Aharonov-Bohm scattering by optical vortices," Phys. Rev. Lett. **87**, 043901-1–4 (2001).
18. M. V. Berry, "Quantal phase factors accompanying adiabatic changes," Proc. R. Soc. London A **392**, 45–57 (1984).
19. R. Simon and N. Mukunda, "Bargmann invariant and the geometry of the Gouy effect," Phys. Rev. Lett. **70**, 880–883 (1993).
20. D. Subbarao, "Topological phase in Gaussian beam optics," Opt. Lett. **20**, 2162–2164 (1995).
21. S. Feng and H. G. Winful, "Physical origin of the Gouy phase shift," Opt. Lett. **26**, 485–487 (2001).
22. J. A. Jones, V. Vedral, A. Ekert, and G. Castagnoli, "Geometric quantum computation using nuclear magnetic resonance," Nature **403**, 869–871 (2000).
23. L.-M. Duan, J. I. Cirac, and P. Zoller, "Geometric manipulation of trapped ions for quantum computation," Science **292**, 1695–1697 (2001).
24. A. B. Ruffin, J. V. Rudd, J. F. Whitaker, S. Feng, and H. G. Winful, "Direct observation of the Gouy phase shift with single-cycle terahertz pulses," Phys. Rev. Lett. **83**, 3410–3413 (1999).
25. R. W. McGown, R. A. Cheville, and D. Grischkowsky, "Direct observation of the Gouy phase shift in THz impulse ranging," Appl. Phys. Lett. **76**, 670–672 (2000).
26. F. Lindner, G. G. Paulus, H. Walther, A. Baltuška, E. Goulielmarkis, M. Lezius, and F. Karusz, "Gouy phase shift for few-cycle-laser pulses," Phys. Rev. Lett. **92**, 113001-1–4 (2004).
27. L. G. Gouy, "Sur une propriété nouvelle des ondes lumineuses," Compt. Rendue Acad. Sci. (Paris) **110**, 1251–1253 (1890).
28. C. R. Carpenter, "Gouy phase advance with microwaves," Am. J. Phys. **27**, 98–100 (1959).
29. J. H. Chow, G. de Vine, M. B. Gray, and D. E. McClelland, "Measurement of Gouy phase evolution by use of mode interference," Opt. Lett. **29**, 2339–2341 (2004).
30. J. Arlt, "Handedness and azimuthal energy flow of optical vortex beams," J. Mod. Opt. **50**, 1573–1580 (2003).
31. B. Luther-Davies, R. Powels, and V. Tikhonenko, "Nonlinear rotation of three-dimensional dark solitons in a Gaussian laser beam," Opt. Lett. **19**, 1816–1818 (1994).
32. F. Flossmann, U. T. Schwarz, and M. Maier, "Optical vortices in a Laguerre-Gaussian LG_1^0 beam," J. Mod. Opt. **52**, 1009–1017 (2005).
33. K. O'Holleran, M. J. Padgett, and M. R. Dennis, "Topology of optical vortex lines formed by the interference of three, four, and five plane waves," Opt. Express **14**, 3039–3044 (2006).
34. M. J. Padgett and L. Allen, "The Poynting vector in Laguerre-Gaussian laser modes," Opt. Commun. **121**, 36–40 (1995).

1. Introduction

Screw dislocations or vortices are classified as one of the categories for topological deformation of fields. They are associated with a topological charge, specified by an integer which determines the accumulated phase change in the closed loop around the dislocation center. In the case of optical beams, the Laguerre-Gaussian (LG) mode LG_p^m is one of the modes of paraxial solutions to the wave equation and has screw phase dislocations. The main character of this mode is that its phase distribution of $m\varphi$ (m; integer), which provides a helical shape for the wavefronts around the beam center with phase singularity. Here, φ is the azimuthal angle and m is the azimuthal index that represents topological charge, that is, the number of 2π cycles in phase about circumference. Another parameter p is the radial index that effectively represents the number of nodal rings about the beam axis. A peculiarity of beams with helical wavefronts lies in the presence of transverse energy circulation, which is termed an optical vortex. The optical vortex carries a well-defined orbital angular momentum (OAM) $m\bar{h}$ per photon [1]. It is distinct from a spin angular momentum which is carried by a circularly-polarized light beam. Such a beam with the OAM recently attracted significant research interest because of its increasing applications, such as high-efficiency laser trapping [2, 3, 4], especially trapping for Bose-Einstein condensates (BECs) [5, 6, 7], microstructure rotation in laser tweezers and spanners [8, 9, 10], and quantum information using multidimensional entangled states [11, 12, 13]. Several nonlinear optical processes have been investigated using LG beams [14, 15], includ-

ing ultrashort pulses [16]. Optical vortex solitons in self-defocusing media demonstrated many common properties with vortices in superfluids and in BECs [17] .

The propagating complex electric field E_{mp} and its slowly-varying envelope u_{mp} of the LG_p^m mode with frequency ω at time t are given by

$$E_{mp}(\rho,\varphi,z,t) = u_{mp}(\rho,\varphi,z)\exp[i(kz-\omega t)], \tag{1}$$

$$\begin{aligned} u_{mp}(\rho,\varphi,z) = \quad & \sqrt{\frac{2p!}{\pi(p+|m|)!}}\left[\frac{\sqrt{2}\rho}{w(z)}\right]^{|m|} L_p^{|m|}\!\left(\frac{2\rho^2}{w(z)^2}\right)\frac{w_0}{w(z)} \\ & \times\exp\left[-\frac{\rho^2}{w(z)^2} - i\frac{k\rho^2}{2R(z)} + im\varphi - i\Phi_{\mathrm{G}}(z)\right], \end{aligned} \tag{2}$$

respectively, where ρ and z denote cylindrical polar coordinates, k is wave number in vacuum, and $L_p^{|m|}(x)$ is the generalized Laguerre polynomial defined by

$$L_p^{|m|}(x) = \sum_{r=0}^{p}(-1)^r\begin{pmatrix} p+|m| \\ p-r \end{pmatrix}\frac{x^r}{r!}. \tag{3}$$

Parameters $R(z)$ and $w(z)$ denote the radius of curvature of wavefronts and the beam size at a propagation distance z, as expressed by

$$R(z) = (z_{\mathrm{R}}^2+z^2)/z, \qquad w(z) = w_0\sqrt{1+z^2/z_{\mathrm{R}}^2}. \tag{4}$$

with the Rayleigh range

$$z_{\mathrm{R}} = kw_0^2/2. \tag{5}$$

The constant w_0 is the beam waist. The parameter Φ_{G} denotes Gouy phase, which is known to be an additional phase shift for a focused and propagated beam, differing from that for a plane wave. It is given by

$$\Phi_{\mathrm{G}}(z) = (2p+|m|+1)\Phi(z) \equiv (2p+|m|+1)\arctan(z/z_{\mathrm{R}}), \tag{6}$$

where $\Phi(z)$ is the fundamental Gouy phase for the Hermite-Gaussian HG_{00} (TEM_{00}) beam. This Gouy phase is observed as an axial phase shift that a converging light beam experiences when it passes through a focal point in propagation. In recent papers, it has been shown that the Gouy phase shift is another manifestation of a general Berry's phase [18, 19, 20, 21], which is an additional geometrical or topological phase acquired by a system after cyclic adiabatic evolution in parameter space. The Berry's phase or geometric phase has been considered to be a promising tool for quantum computation [22, 23].

Recently, for single-cycle terahertz pulses [24, 25] or few-cycle femtosecond laser pulses [26], the Gouy phase shift has been directly observed both as a change of carrier-envelope phase. However, for continuous wave (cw) or many-cycle pulses, experimental observations of the Gouy phase shift have been based on interferometric measurements [27, 28]. A novel method demonstrated more recently was still relied on an interferometric measurement, where the Gouy phase shift was observed as a phase difference between TEM_0 and TEM_1 modes in one dimension, using a spatial mode interference-locking technique [29].

In the present paper, we present direct experimental observation of the Gouy phase shift for a propagated and focused LG beam by introducing an asymmetric defect. Having the ability to

determine the value of the Gouy phase shift at a propagation distance, the technique that we used here is simple and useful without need of a conventional interference method. The present paper is organized as follows. First, the experimental observation of the Gouy phase shift for LG beams is described. Second, the experimental results are analyzed using slowly-varying envelope functions.

2. Experimental setup

An LG beam or an optical vortex was generated using two-dimensional-programmable spatial light modulator (SLM; HOLOEYE LC-R 2500, pixel number 1024×768, pixel size of 19 μm×19 μm) as shown in Fig. 1(a). The light source used was a linearly-polarized cw He-Ne laser (632.8 nm). The beam from the laser was reflectively diffracted by a hologram patterned on the SLM. A spiral pattern (typically as shown in Fig. 1(b)) on SLM enables us to eliminate easily the 0th-order diffraction beam using a configuration of optics and thus generate a well-defined LG beam with topological charge of m. For example, Fig. 1(c) shows the intensity profile of LG ($m = 10$ and $p = 0$) beam. Observation of only one ring guaranteed that the generated LG beam was in the well-defined $p = 0$ mode. In the present study, we introduced an asymmetric defect (defect angle $\pi/3$) of the hologram by SLM pattern like Fig. 1(d). This defect broke the circular symmetry. For the diffracted beam from the hologram, its beam profile becomes like a character of 'C' shown as Fig. 1(e). To clarify the beam profile evolution originating in the Gouy phase shift under propagation, the beam was focused by a convex lens with a focal length of $f = 1000$ mm after diffraction from the hologram and its transverse intensity profile was monitored by a charge-coupled device (CCD) camera at a propagation distances z as shown in Fig. 1(a). Here, z is the coordinate along the propagation direction and the focal point was put to be $z = 0$.

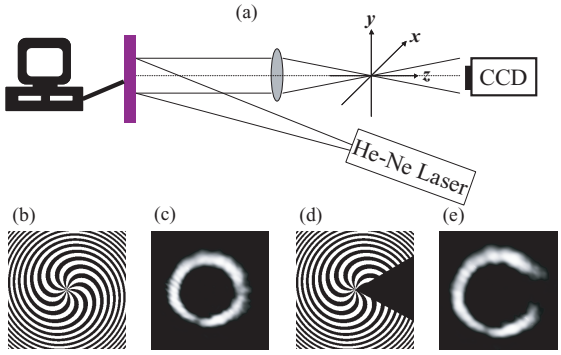

Fig. 1. (a) Experimental setup for spatial evolution measurement of a modified LG beam with an asymmetric defect, (b) a normal spiral hologram pattern, (c) a pure LG beam, (d) a spiral hologram pattern with an asymmetric defect (defect angle $\pi/3$), and (e) a modified LG beam with an asymmetric defect.

3. Experimental results

We introduced an asymmetric defect to beams with $(m, p) = (0, 0)$ and $(\pm 10, 0)$ by modifying hologram patterns. The spatial evolution of modified, that is, 'C'-figured beams with $m = 0$ and ± 10 was investigated. Figure 2 shows their intensity profiles at $z = -55$, -15, 0, +15, and 55 cm. Only at $z = +55$ cm, the 0th-order diffraction beams by SLM were not optically eliminated as shown at the center in Figs. 2(a) and 2(b).

For a modified-LG beam with $(m,p)=(+10,0)$, the introduced defect was rotated along the ring from $\varphi=0$ direction to $\varphi\simeq+\pi$ direction with propagation distance z. The rotation was in the counterclockwise sense on CCD when observed from $+z$-direction. On the contrary, for a modified-LG beam with $(m,p)=(-10,0)$, the defect was rotated in the clockwise sense, from $\varphi=0$ direction to $\varphi\simeq-\pi$ direction, with increasing distance z.

In good contrast to these results, for a modified-LG beam with $(m,p)=(0,0)$, which corresponds to the modified Hermite-Gaussian HG_{00} mode, it is definitely found that the beam profile at $z>0$ after passing the focal point was spatially inverted from that before the focal point at $z<0$. While the defect on the ring of the modified-LG beam with $(m,p)=(0,0)$ was in the direction of $\varphi=0$ in $z<0$ region (before the focal point), it was in the direction of $\varphi=\pm\pi$ in $z>0$ region (after the focal point). The detailed observation showed that the asymmetric defect was rotated in both clockwise and counterclockwise senses.

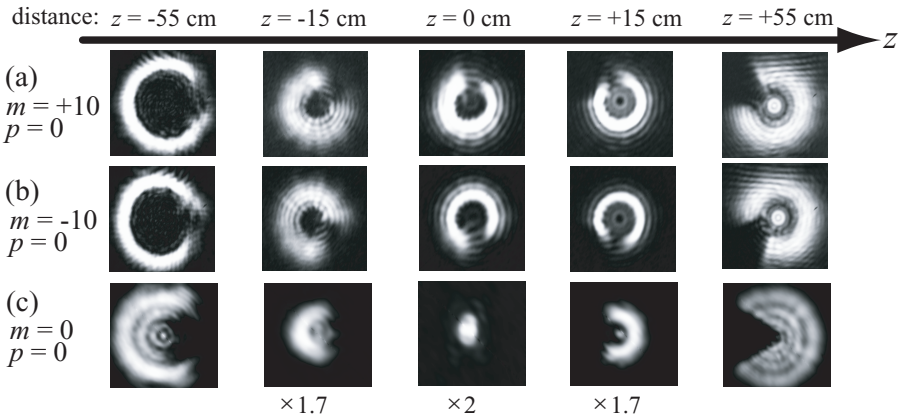

Fig. 2. Experimantally-observed spatial evolution of modified LG beams with an aymmetric defect for (a) $(m,p)=(+10,0)$, (b) $(m,p)=(-10,0)$ and (c) $(m,p)=(0,0)$. The intensity profiles at $z=-15,0$, and $+15$ cm are magnified 1.7, 2, and 1.7 times, respectively.

We also investigated the spatial evolution of modified-LG beams with different $(m,0)$ values. The rotation direction was found to be determined by the sign of the topological charge m. Namely, intensity profiles of modified-LG beams were rotated counterclockwise for $m>0$ and clockwise for $m<0$ when observed on CCD (from $+z$-direction), as indicated in Figs. 2(a) and 2(b), which was qualitatively in accordance with the result in Ref. [30]. Quantitatively the average azimuthal angles $\varphi_{\rm D}$ of the defect in the modified-LG beam ring for $m=\pm10$ are plotted in Fig. 3. This behavior well agreed with the dependence of the fundamental Gouy phase $\mathrm{sgn}(m)\Phi(z)=\mathrm{sgn}(m)\arctan(z/z_{\rm R})$ on propagation distance z, where

$$\mathrm{sgn}(m)=\begin{cases}+1, & m>0,\\ -1, & m<0.\end{cases} \tag{7}$$

Hence, while the absolute value of the rotation angle was $\sim\pi$ independent of the topological value m (in $p=0$ cases), the rotation direction only depended on the sign of m. This rotational property of the defect is similar to that for dark solitons with weak nonlinearity [31]. In addition, we confirmed that the fundamental Gouy phase shift under propagation from the convex lens position to focal point was less than $\pi/2$, thanks to a finite propagation distance. The origin of this feature of modified-LG beams will be discussed in the next section.

In addition, we investigated the 3-dimensional (3D) trajectory [32, 33] of the asymmetric

defect as well as rotation direction. Figure 4 shows the trajectories of the defect position projected on $x-y$ plane as a function of propagation distance z, for modified LG beam with $(m,p)=(+10,0)$ and $(-10,0)$. The paths swept out by the defect are described as straight lines and the defect makes a uniform motion.

The advantages of our technique are not only direct Gouy-phase shift observation, but also the capability to evaluate the Rayleigh length z_{R} and beam waist w_0. They are fundamental and significant parameters. However, it has been difficult to evaluate them directly from intensity profiles of LG beams, owing to their peculiar shape with central phase singularity. It has been a sharp contrast to the case for HG_{00} beams. By fitting our experimental results to Eq. (6), the Rayleigh length z_{R} and beam waist w_0 were evaluated to be 184 mm and 190 μm, respectively. Thus our technique is a powerful tool to obtain detailed information for LG beams.

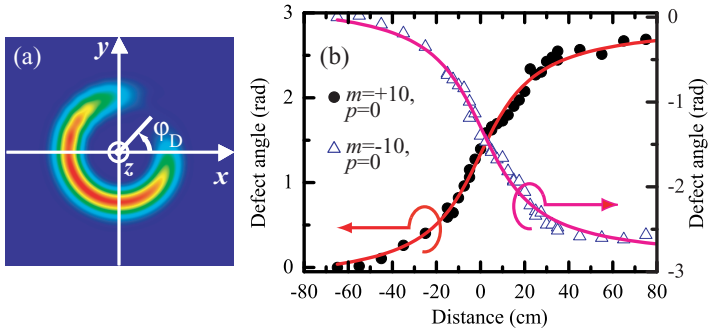

Fig. 3. (a) Schematic drawing for an intensity profile of a modified LG beam with an aymmetric defect with the coordinates x,y,z, and average defect angle φ_{D} when observed from $+z$-direction on CCD. (b) Dependence of observed defect angle φ_{D} on the propagation distance z for modified LG beams with $(m,p)=(+10,0)$ and $(-10,0)$.

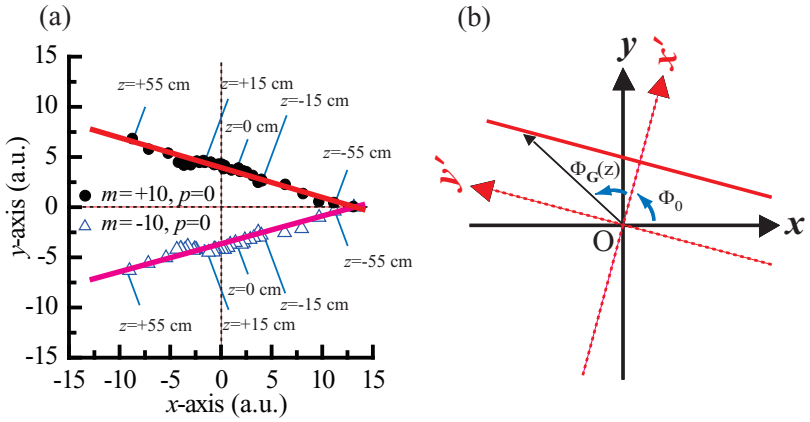

Fig. 4. (a) 3D trajectories of the asymmetric defect for modified LG beams with $(m,p)=(+10,0)$ and $(-10,0)$ projected on $x-y$ plane as a function of propagation distance z. (b) Relationship between coordinates x,y and x',y'. (x',y',z) coordinates are obtained from (x,y,z) coordinates by a roation of Φ_0 around the z axis. In our experimental configuration, we put $\varphi_{\mathrm{D}}=0$ at $z=-65$ cm with the initial phase Φ_0.

4. Discussions

4.1. Rotation of the defect

First, we discuss the rotation of the asymmetric defect in the *x*-*y* plane. The modified-LG beam with an asymmetric defect is not expressed by a pure LG mode $u_{mp}(\rho,\varphi,z)$ but by a superposition of LG modes.

The slowly-varying envelope $\Psi^{\mathrm{C}}_{mp}(\rho,\varphi,z)$ of the modified ('C'-figured) LG beam with an asymmetric defect can be approximately expressed by

$$\Psi^{\mathrm{C}}_{mp}(\rho,\varphi,z) = u_{mp}(\rho,\varphi,z)\{1-\exp[-\varphi^2/2(\delta\varphi_{\mathrm{D}})^2]\}, \tag{8}$$

where $\delta\varphi_{\mathrm{D}}$ is the effective angle of the defect area ($1/e$-intensity angle). The slowly-varying envelope $\Psi^{\mathrm{C}}_{mp}(\rho,\varphi,z)$ is also described as a superposition of pure LG modes by

$$\Psi^{\mathrm{C}}_{mp}(\rho,\varphi,z) = \sum_{p'=0}^{\infty}\sum_{m'=-\infty}^{\infty} C_{m'p'}u_{m'p'}(\rho,\varphi,z). \tag{9}$$

Here, $C_{m'p'}$ is an expansion coefficient which corresponds to the overlapping integral,

$$C_{m'p'} = \frac{1}{w_0^2}\int_0^{\infty}\mathrm{d}\rho\,\rho\int_{-\pi}^{\pi}\mathrm{d}\varphi\,u^*_{m'p'}(\rho,\varphi,z)\Psi^{\mathrm{C}}_{mp}(\rho,\varphi,z), \tag{10}$$

which can be shown to be constant independent of z.

The intensity profile of the modified LG beam at a propagation distance z is given by

$$\begin{aligned}
&\left|\Psi^{\mathrm{C}}_{mp}(\rho,\varphi,z)\right|^2 \\
&= \sum_{p''=0}^{\infty}\sum_{m''=-\infty}^{\infty}\sum_{p'=0}^{\infty}\sum_{m'=-\infty}^{\infty} C^*_{m''p''}C_{m'p'}u^*_{m''p''}(\rho,\varphi,z)u_{m'p'}(\rho,\varphi,z) \\
&= \frac{2}{\pi}\frac{w_0^2}{w(z)^2}\exp\left[-\frac{2\rho^2}{w(z)^2}\right]\sum_{p''=0}^{\infty}\sum_{m''=-\infty}^{\infty}\sum_{p'=0}^{\infty}\sum_{m'=-\infty}^{\infty} C^*_{m''p''}C_{m'p'}\sqrt{\frac{p'!\,p''!}{(p'+|m'|)!(p''+|m''|)!}} \\
&\quad\times\left[\frac{\sqrt{2}\rho}{w(z)}\right]^{|m'|+|m''|} L_{p'}^{|m'|}\!\left(\frac{2\rho^2}{w(z)^2}\right)L_{p''}^{|m''|}\!\left(\frac{2\rho^2}{w(z)^2}\right) \\
&\quad\times\exp\left\{i(m'-m'')\varphi - i[2(p'-p'')+|m'|-|m''|]\Phi(z)\right\} \\
&\equiv \frac{4}{\pi}\frac{w_0^2}{w(z)^2}\exp\left[-\frac{2\rho^2}{w(z)^2}\right](A+B+C+D+E),
\end{aligned} \tag{11}$$

where terms $A, B, C, D,$ and E are defined by

$$A = \sum_{p'=0}^{\infty}\sum_{m'=-\infty}^{\infty}\left|C_{m'p'}\right|^2\frac{p'!}{(p'+|m'|)!}\left[\frac{\sqrt{2}\rho}{w(z)}\right]^{2|m'|}\left[L_{p'}^{|m'|}\!\left(\frac{2\rho^2}{w(z)^2}\right)\right]^2, \tag{12}$$

$$\begin{aligned}
B &= \sum_{p'=0}^{\infty}\sum_{m'=-\infty}^{\infty}\sum_{m''<m'} C^*_{m''p'}C_{m'p'}\frac{p'!}{\sqrt{(p'+|m'|)!(p'+|m''|)!}}\left[\frac{\sqrt{2}\rho}{w(z)}\right]^{|m'|+|m''|} \\
&\quad\times L_{p'}^{|m'|}\!\left(\frac{2\rho^2}{w(z)^2}\right)L_{p'}^{|m''|}\!\left(\frac{2\rho^2}{w(z)^2}\right)\cos\left[(m'-m'')\varphi-(|m'|-|m''|)\Phi(z)\right],
\end{aligned} \tag{13}$$

$$C = \sum_{p'=0}^{\infty}\sum_{m'=-\infty}^{\infty}\sum_{p''<p'} C^*_{m'p''}C_{m'p'}\sqrt{\frac{p'!\,p''!}{(p'+|m'|)!(p''+|m'|)!}}$$

$$\times \left[\frac{\sqrt{2}\rho}{w(z)}\right]^{2|m'|} L_{p'}^{|m'|}\left(\frac{2\rho^2}{w(z)^2}\right) L_{p''}^{|m'|}\left(\frac{2\rho^2}{w(z)^2}\right) \cos\left\{2(p'-p'')\Phi(z)\right\}, \tag{14}$$

$$D = \sum_{p'=0}^{\infty}\sum_{m'=-\infty}^{\infty}\sum_{p''<p'}\sum_{m''<m'} C^*_{m''p''}C_{m'p'}\sqrt{\frac{p'!\,p''!}{(p'+|m'|)!(p''+|m''|)!}}$$
$$\times \left[\frac{\sqrt{2}\rho}{w(z)}\right]^{|m'|+|m''|} L_{p'}^{|m'|}\left(\frac{2\rho^2}{w(z)^2}\right) L_{p''}^{|m''|}\left(\frac{2\rho^2}{w(z)^2}\right)$$
$$\times \cos\left\{(m'-m'')\varphi - [2(p'-p'')+|m'|-|m''|]\Phi(z)\right\}, \tag{15}$$

$$E = \sum_{p'=0}^{\infty}\sum_{m'=-\infty}^{\infty}\sum_{p''>p'}\sum_{m''<m'} C^*_{m''p''}C_{m'p'}\sqrt{\frac{p'!\,p''!}{(p'+|m'|)!(p''+|m''|)!}}$$
$$\times \left[\frac{\sqrt{2}\rho}{w(z)}\right]^{|m'|+|m''|} L_{p'}^{|m'|}\left(\frac{2\rho^2}{w(z)^2}\right) L_{p''}^{|m''|}\left(\frac{2\rho^2}{w(z)^2}\right)$$
$$\times \cos\left\{(m'-m'')\varphi - [2(p'-p'')+|m'|-|m''|]\Phi(z)\right\}. \tag{16}$$

for a modified LG_p^m beam.

Here, we discuss the spatial evolution of propagating LG beams for three typical cases, (i) $m \neq 0$ ($|m| \gg 1$), $p = 0$, (ii) $m = 0, p = 0$, and (iii) $m \neq 0$ ($|m| \gg 1$), $p \neq 0$ ($p \gg 1$). Distributions of $|C_{mp}|^2$ as a function of indices m and p for modified LG beams, as expressed by Eq. (10), are depicted in Fig. 5. Figure 6 shows calculated spatial evolution of modified LG beams for three cases, using Eq. (11).

4.1.1. (i) $m \neq 0$ ($|m| \gg 1$) and $p = 0$ case

In case $p = 0$, that is, for Ψ^{C}_{m0}, the pair of indices (m', p') of the expansion coefficients $C_{m'p'}$ (also (m'', p'') of the expansion coefficients $C_{m''p''}$) are distributed around $(m, 0)$. For example, the distribution of $|C_{m'p'}|^2$ for $m = 10$ and $p = 0$ is shown in Fig. 5(a). Thus, we can see that the term including $|C_{m0}|^2$ in A and terms in B in Eq. (11) are the most dominant. The former terms are independent of φ. The latter terms have have a factor of $\cos\Delta \equiv \cos[(m'-m'')\varphi - (|m'| - |m''|)\Phi(z)]$. When $p = 0$, terms of C and D are negligible. Terms of E are estimated to be small though they smear the intensity profile. When $|m| \gg 1$, the index m' and m'' are distributed mainly around m. Thus, we put

$$m' = m + \delta m' \quad (|\delta m'| \ll |m|),$$
$$m'' = m + \delta m'' \quad (|\delta m''| \ll |m|).$$

The factor $\cos\Delta$ is therefore given by

$$\cos\Delta = \cos\{(\delta m' - \delta m'')[\varphi - \mathrm{sgn}(m)\Phi(z)]\}. \tag{17}$$

Hence, the defect of the propagating beam along z-axis, which is expressed by $\varphi - \mathrm{sgn}(m)\Phi(z) = \text{const.}$, is rotated counterclockwise or clockwise depending on the sign of m, namely, $m > 0$ or $m < 0$, respectively, as shown in Figs. 6(a) and 6(b). when observed on CCD.

4.1.2. (ii) $m = 0$ and $p = 0$ case

In this case, the pair of indices (m', p') of the expansion coefficients $C_{m'p'}$ are distributed around $(0, 0)$. For example, the distribution of $|C_{m'p'}|^2$ for $m = 0$ and $p = 0$ is shown in Fig. 5(c). Thus

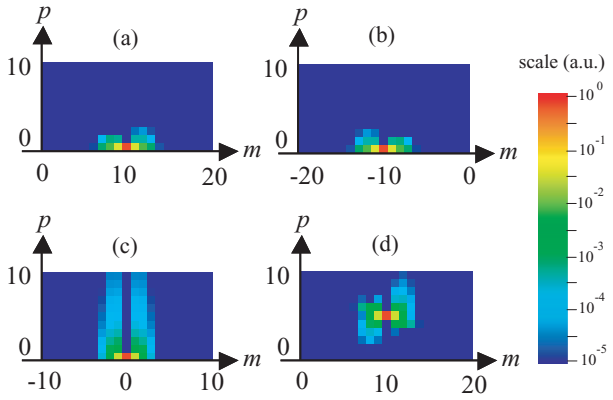

Fig. 5. Distributions of $|C_{mp}|^2$ as a function of indices m and p for modified LG beams with (a) $(m,p)=(+10,0)$, (b) $(m,p)=(-10,0)$ (c) $(m,p)=(0,0)$ and (d) $(m,p)=(+10,5)$.

the phase in Eq. (17) is given by

$$\begin{aligned}\Delta &= (\delta m' - \delta m'')\varphi - (|\delta m'| - |\delta m''|)\Phi(z) \\ &= \begin{cases} (\delta m' - \delta m'')[\varphi - \Phi(z)], & \delta m' > 0, \delta m'' > 0, \\ (\delta m' - \delta m'')\varphi - (\delta m' + \delta m'')\Phi(z), & \delta m' > 0, \delta m'' < 0, \\ (\delta m' - \delta m'')[\varphi + \Phi(z)], & \delta m' < 0, \delta m'' < 0, \\ (\delta m' - \delta m'')\varphi + (\delta m' + \delta m'')\Phi(z), & \delta m' < 0, \delta m'' > 0. \end{cases} \end{aligned} \tag{18}$$

It is found that, in this case in good contrast to (i), the defect in the ring is rotated simultaneously in clockwise and counterclockwise senses. Both clockwise- and counterclockwise-rotated defects are broadened depending on the distribution of $\delta m'$ and $\delta m''$. It is clearly indicated in Figs. 2(c) and 6(c).

4.1.3. (iii) $m \neq 0$ ($|m| \gg 1$) and $p \neq 0$ ($p \gg 1$) case

In this case, the pair of indices (m', p') of the expansion coefficients $C_{m'p'}$ are distributed around (m,p). For example, the distribution of $|C_{m'p'}|^2$ for $m=+10$ and $p=+5$ is shown in Fig. 5(d). It is noted that unlike $p=0$ case, $C_{m'p'}$ are distributed in the region of $p' < p$. Thus, the situation is much complicated owing to contribution of D terms as well as A, B and E terms. The sense of rotation is still determined by the sign of m. Although D and E terms are small, they affect the intensity profile through Gouy phase shift including p' and p'' values. The former makes the defect rotate more than π, while the latter less than π. Hence, the intensity profile has $(p+1)$-rings and rotational angles of the defects in the rings depend on the radial coordinate ρ. For example as shown in Fig. 6(d), when the rotated angle $\varphi_{\rm rot}$ in the region of $0 < |\varphi_{\rm rot}| < \pi/2$, inner rings rotates faster than outer rings; in the region of $\pi/2 < |\varphi_{\rm rot}| < \pi$, vice versa. However, averages of total rotational angles are π for all rings, reflecting the Gouy phase shift.

It is noted that the present technique is more effective for larger $|m|$, because of the radial dependence for LG modes. The radius of maximum amplitude $\rho_{\rm max}$ is expressed by $\rho_{\rm max} = \sqrt{m/2}\,w(z)$ for $p=0$. Hence, for larger $|m|$, the displacement of $\rho_{\rm max}$ between $m+\delta m$, m and/or $m-\delta m$ is neglected, while the displacement of $\rho_{\rm max}$ become larger for smaller $|m|$ ($\simeq$ 1), resulting in less spatial overlapping of constituent LG modes.

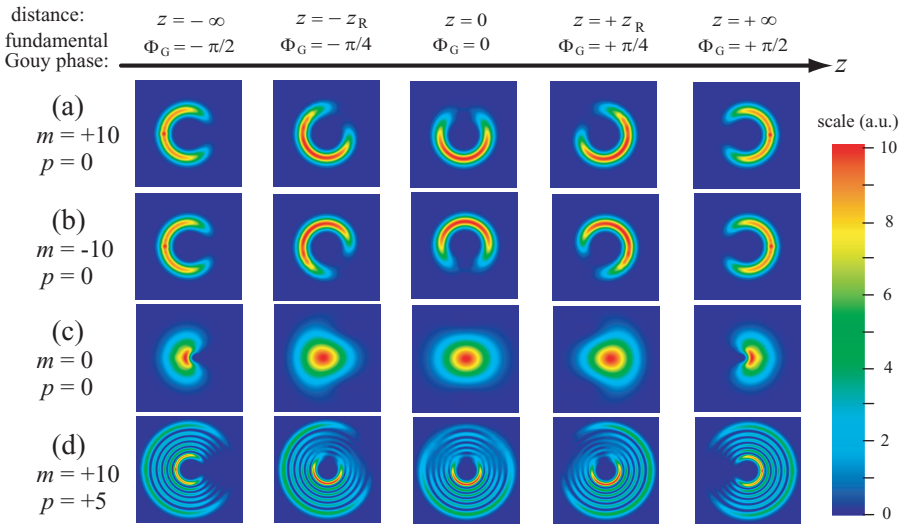

Fig. 6. Calculated spatial evolution of modified LG beams with an aymmetric defect for (a) $(m,p)=(+10,0)$, (b) $(m,p)=(-10,0)$, (c) $(m,p)=(0,0)$ and (d) $(m,p)=(+10,+5)$ at propagation distances of $z=-\infty,-z_R,0,-z_R$, and $+\infty$. Dimensions of beams are scaled by $w(z)$.

4.2. 3D trajectory of the defect

Second we discuss the 3D trajectory of the asymmetric defect. Experimental results showed the asymmetric defect describes the straight and uniform path. This fact indicates that there is no additional force to the defect. Moreover, we can interpret that the fundamental Gouy phase shift corresponds to the defect rotation angle around the phase singular point of the vortex, that is, $(x,y)=(0,0)$.

Now we analyze this 3D trajectory. The effective radius ρ_D of the asymmetric defect is expressed as $\sqrt{m/2}\,w(z)$ in the case where $p=0$. As shown in Fig. 4(b), we put the azimuthal angle of the defect to be $\Phi_G+\Phi_0$. Thereby the effective defect position in $x-y$ plane is expressed by

$$x(z)=w(z)\sqrt{\frac{m}{2}}\cos(\Phi_G+\Phi_0),\qquad y(z)=w(z)\sqrt{\frac{m}{2}}\sin(\Phi_G+\Phi_0). \tag{19}$$

With the help of the definition of $w(z)$ in eq. (4), we obtained that

$$\begin{bmatrix} x \\ y \end{bmatrix}=\begin{bmatrix} \cos\Phi_0 & -\sin\Phi_0 \\ \sin\Phi_0 & \cos\Phi_0 \end{bmatrix}\begin{bmatrix} x' \\ y' \end{bmatrix}, \tag{20}$$

where x',y' are coordinates rotated by angle Φ_0 around z-axis from (x,y) coordinates given by

$$x'(z)=w_0\sqrt{\frac{m}{2}},\qquad y'(z)=w_0\sqrt{\frac{m}{2}}\frac{z}{z_R}. \tag{21}$$

Thus, it is derived that the trajectory of the defect describes the straight line and makes a uniform motion. Extending this context to other LG beams, it was found that trajectories of the defect (effective position) for any LG_p^m modes have the same properties.

4.3. comparison with other analyses

Padgett *et al.* have calculated and investigated the Poynting vector of eigenmodes LG_p^m [34]. They indicated that the rotation of the Poynting vector corresponds to the Gouy phase shift when p=0, and the Poynting vector of the inner ring is faster than that of outer ring(s) when $p > 0$. The intensity profile of knife-edged LG mode with small m was experimentally investigated and its behavior was investigated [30]. The knife-edged portion was azimuthally traversed owing to the Gouy phase shift, however it was difficult to estimate Gouy phase shift from their intensity profile. It was because of position ambiguity of the phase singular point of $(x,y) = (0,0)$ resulting form their defect angle of π. Furthermore, the deformation of the profile became severe for smaller m.

It should be noted that the calculated Poynting vector in Ref. [34] is not appropriate to the LG beam with an asymmetric defect, or that it is applicable only in short range spatial evolution. It is attributed to the fact that the LG beam with an asymmetric defect is not a pure LG mode but is expressed by a superposition of LG modes. For example, there are six rings with a defect in Fig. 6(d) at $z = -\infty$, Although the rings rotate according to the Poynting vector in $z < 0$ region, the defect blurs out at $z = 0$. This indicates that rings do not rotate independently with each other. Moreover, the defect disappears at $z = 0$ in the case of small m, which cannot be expected by only considering in the Poynting vector.

Here we discussed the case of $p = 0$ and large m introducing the appropriated defect angle of about $\pi/3$, only where it is optimal to evaluate Gouy phase shift. Thus our technique and analysis of the spatial evolution of optical vortices with an asymmetric defect is significant.

5. Conclusion

In conclusion, we directly observed the Gouy phase shift by measuring the intensity profiles of an LG_p^m beam with an asymmetric defect when it was propagated around at the focal point. We quantitatively found that the rotation profile of a modified LG_p^m beam manifests the Gouy phase effect where the rotation direction depends on only the sign of topological charge m (counterclockwise for $m > 0$; clockwise for $m < 0$ when observed from $+z$-direction). This profile measurement method of an LG beam with an asymmetric defect is a simple and useful technique for obtaining the information of fundamental Gouy phase shift, without need of a conventional interference method using two beams. Moreover, we analyzed the spatial evolution of the asymmetric defects in LG beams. A modified LG_p^m beam with an asymmetric defect is expressed by the superposition of pure LG modes whose indices are distributed mainly around (m, p). This superposition well explains the rotational evolution of the defect in space. In addition, we showed experimentally and theoretically that the 3D trajectory of the defect describes a uniform straight line.

Acknowledgments

The authors would like to thank S. Tanda for his useful discussion and encouragement. This work was partially supported by Grant-in-Aid for the 21st Century COE program on “Topological Science and Technology” and Grant-in-Aid for Exploratory Research, 2005-2006, No. 17656020, from the Ministry of Education, Culture, Sports, Science and Technology of Japan.